Semiempirical calculations of the zero-degree-Kelvin isotherm in metals

H. Szichman and A. D. Krumbein
Plasma Physics Department, Soreq Nuclear Research Center, Yavne, Israel
(Received 9 April 1985)

A phenomenological model has been devised for calculating the cold compression curves of metals up to the 10-TPa pressure region. The nuclear Grüneisen coefficient can also be correctly computed using this model. Shock Hugoniot curves were calculated for several metals using these cold compression curves to which the ion and electron thermal contributions were added. The results gave excellent agreement with experimental results for Pb, W, and Cd when the electron thermal portion is computed according to the Thomas-Fermi-Khirzhnits model. For Al, Cu, Fe, and Mo other electron thermal models must be used to give agreement with experimental results.

I. INTRODUCTION

Recently it has become possible to measure pressures in the TPa range using a variety of new methods, from underground nuclear explosions[1] to large pulsed lasers,[2,3] and including such novel means as rail guns.[4] In general these experiments are of the impedance-matching type which require for their interpretation a fairly exact knowledge of the equation of state (EOS) of some reference material. As the pressures attained have climbed to the TPa range, the reference EOS has had to be based more and more on theoretical calculations and/or extrapolation from better-known pressure regions. Particularly problematical has been the computation of the cold compression curve or zero-degree-Kelvin isotherm.[5]

One of the standard sources of reference EOS data for impedance-matching experiments has been the Los Alamos Scientific Laboratory (LASL) SESAME tables.[6] These tables were generated for most materials using a phenomenological model due to Barnes[7] for computing the cold curves and the temperature-dependent Thomas-Fermi-Dirac (TFD) theory[8] for calculating the electron thermal contribution. However, comparisons between theoretical Hugoniot curves calculated from the SESAME tables and experimental points recently obtained by Ragan[1,9,10] showed that the validity of this SESAME EOS model appears to be limited to the region below 100–200 GPa. Agreement with experiment was improved for some metals by using recent additions to the SESAME library.[11] However, for practical applications, particularly to impedance-matching experiments on metals, it is of interest to determine a more realistic phenomenological model for the cold compression curves which can be used in matching the experimental data above 200 GPa.

In this paper we present a semiempirical model for the cold curve which is based on an analytical interpolation between a modified version of the Barnes model and the quantum statistical model (QSM) of the isolated atom.[12,13] This interpolation, which is valid for pressures in the TPa range, yields only two free parameters which have to be fitted to match the experimental results. This is in contrast to most of the semianalytical expressions found in the literature[5] which have, in general, a greater number of free parameters to be fitted with experimental data. Due to the spread in the latter, these various semianalytic expressions, while in reasonable agreement within the interpolation interval, display large differences in their asymptotic behavior, i.e., outside of the experimental region. We use this model to calculate the Hugoniot curves of various metals employing in the calculation one of two theoretical models for computing the electron thermal contribution. Excellent agreement with experiment is obtained.

II. THE PHENOMENOLOGICAL MODEL

The original Barnes formulation[7] for the cold curve is given by

$$P_c = a\eta^{2/3}(\eta e^{b_r \nu} - e^{b_a \nu}) , \tag{1}$$

where $\nu = 1-\eta^{-1/3}$, η being the compression ratio ρ/ρ_0. a and b_r are chosen so as to make the repulsive term of Eq. (1) reproduce the pressure as given by one of the known statistical models (Thomas-Fermi, TFD, or QSM) while b_a can be determined from the experimental bulk modulus B_0 by

$$B_0 = \left.\frac{\partial P_c}{\partial \eta}\right|_{\eta=1} = \frac{a}{3}(3+b_r-b_a) . \tag{2}$$

This formulation appears to suffer from several difficulties.

(1) For most of the materials cited by Barnes in Ref. 7 there are significant differences between the normal Grüneisen coefficient Γ_0 and the theoretical value derived from Eq. (1) by use of the Dugdale-MacDonald[14] (DM) formula, as shown in Ref. 7.

(2) Kalitkin and Kuz'mina,[12] in developing their QSM, performed an analytical interpolation of the numerical solutions of the Khirzhnits energy equation[15] for highly compressed matter and showed that there is apparently an additional quadratic term in the argument of the exponential decay term in Eq. (1). Incidentally, this is not totally unexpected as the Barnes expression was derived from an analogy to the Morse diatomic potential model which is valid for molecules and crystals in the normal pressure

range.

(3) The TFD and the QSM theories[13] predict a correction to the pressure with a dominant term which scales as the electron density on the atom boundary raised to the power of $\frac{4}{3}$. This power law results from the exchange forces which are accounted for in these models. It was shown by More[13] that within the framework of the QSM this electron density is almost proportional to the average charge density in the atom, and then the correction term scales as $\eta^{4/3}$. Similar behavior is also predicted by electron-gas perturbation theory.[13] The $\eta^{4/3}$ power law at high compressions is in contrast to the $\eta^{2/3}$ law in the crystal state, Eq. (1). The transition between these two correction terms could be taken into account, as Barnes did, by using the predicted pressure of the TFD, rather than from the Thomas-Fermi model, in describing the repulsive term and assuming that for increasing compression this term predominates over the Morse diatomic correction. However, this method does not appear to be adequate as it determines the behavior of the cold curve at high pressures by extrapolation of numerical relations for the normal state where the TFD model is clearly not correct.

As an alternative, a phenomenological model for the 0-K pressure isotherm is proposed which is composed of the difference between repulsive and attractive terms, viz.,

$$P_c = P_{\mathrm{QSM}} - \delta \ . \tag{3}$$

The positive term, P_{QSM}, is derived from the respective repulsive term in the QSM theory for the pressure (as given in Ref. 12) and δ is defined as

$$\delta = \begin{cases} A_o \eta^{2/3} \exp(-B_a \eta^{-1/3} - B_g \eta^{-2/3}) \ , & \eta \le \eta_1 \\ \sum_{i=1}^{4} A_i \eta^{i/3} \ , & \eta_1 < \eta < \eta_2 \\ \delta_{\mathrm{QSM}} \ , & \eta \ge \eta_2 \ . \end{cases} \tag{4}$$

Here δ_{QSM} is the attractive term in the QSM model[12] and η_1 and η_2 are the boundaries of the interpolation region. The maximum degree of the polynomial in the interpolation region is $\frac{4}{3}$ because of theoretical limitations. The number of polynomial coefficients used in the model is the minimum number required to fulfill the continuity conditions for the correction term δ and its first derivative at the boundaries η_1 and η_2 of the interpolation region, viz.,

$$\begin{aligned} \delta(\eta_j) &= \sum_i A_i \eta_j^{i/3} \ , \\ 3\eta_j \delta'(\eta_j) &= \sum_i A_i i \eta_j^{i/3} \end{aligned} \tag{5}$$

with $j = 1,2$. η_1 and η_2 are the two parameters which are to be fitted with the experimental data. We thus have a system of four linear equations in four unknowns. For fixed values of η_1 and η_2 and known values of the atomic number Z, the atomic volume V_0, and the constants A_0, B_a, and B_g in the Morse correction term, the polynomial coefficients A_i can be calculated from Eq. (5). Moreover, A_0, B_a, and B_g are related to V_0, B_0, and Γ_0 by the boundary conditions of P_c at $\eta = 1$, viz.,

$$\begin{aligned} &P_c(1) = 0 \ , \\ &\left. \frac{\partial P_c}{\partial \eta} \right|_{\eta=1} = B_0 \ , \\ &\left. \frac{\partial^2 P_c}{\partial \eta^2} \right|_{\eta=1} = 2B_0(\Gamma_0 + \tfrac{1}{3}\tau_g) \ . \end{aligned} \tag{6}$$

The last equation is obtained as a result of theoretical considerations linking the Grüneisen coefficient to the cold compression curve.[5] In this equation τ_g is a parameter which varies according to the lattice configuration and can vary from -1 to $+1$.

The constant A_0 is obtained by way of the first equation in (6), viz.,

$$A_0 = P_{\mathrm{QSM}}(V_0) \exp(B_a + B_g) \ , \tag{7}$$

where B_a and B_g are found from the remaining equations of (6). They can be written in the following form:

$$\begin{aligned} B_g &= \frac{9B_0}{P_{\mathrm{QSM}}(V_0)}(\Gamma_0 + \tfrac{1}{3}\tau_g) \\ &\quad - \frac{(5+\alpha+2\beta)^2 - 4\alpha - 10\beta - 13 - \epsilon^2}{2} \ , \\ B_a &= \epsilon - 2B_g \ , \end{aligned} \tag{8}$$

where[12]

$$\begin{aligned} P_{\mathrm{QSM}}(V_0) &= \frac{1}{5}\frac{e^2 a_0}{V_0^{5/3}}(3\pi^2)^{2/3} Z^{5/3} \exp[-(\alpha+\beta)] \ , \\ \epsilon &= 3\left[1 - \frac{B_0}{P_{\mathrm{QSM}}(V_0)}\right] + \alpha + 2\beta \ , \\ \alpha &= 0.3225 R_0 Z^{(0.495 - 0.039 \log_{10} Z)} \ , \\ \beta &= \tfrac{5}{3} R_0^2 [0.068 + 0.078 \log_{10} Z - 0.086 (\log_{10} Z)^2] \ . \end{aligned} \tag{9}$$

The constants here, besides those given previously, are

$$V_0 = 1.660\,420\,7 A/\rho_0 \ \text{Å}^3 \ ,$$

where A is the atomic weight, and

$$R_0 = \frac{1}{a_0}\left[\frac{3}{4\pi} V_0\right]^{1/3} \ ,$$

where $a_0 = \hbar^2/me^2$ is the Bohr radius.

The internal energy along the 0-K isotherm is obtained from known thermodynamic relations, viz.,

$$E_c(\eta) = V_0 \int_1^{\eta} P_c(x) \frac{dx}{x^2} \ . \tag{10}$$

This splits up, depending on the values of δ from Eq. (4), into

$$E_c(\eta)=\begin{cases} V_0\int_1^{\eta} P_c(x)\dfrac{dx}{x^2}\ , & \eta\le\eta_1 \\ E_c(\eta_1)+V_0\int_{\eta_1}^{\eta} P_c(x)\dfrac{dx}{x^2}\ , & \eta_1<\eta<\eta_2 \\ E_c(\eta_2)+V_0\int_{\eta_2}^{\eta} P_c(x)\dfrac{dx}{x^2}\ , & \eta>\eta_2\ . \end{cases} \tag{11}$$

The internal energy is best computed by numerical integration of Eqs. (11) since there is no simple analytical solution. This is due to the quadratic term in the exponential decay found in the expression for the pressure.

III. HUGONIOT CURVES AND THERMAL CONTRIBUTIONS TO THE EQUATION OF STATE

The best method of testing the validity of the 0-K isotherms given by Eqs. (3)–(9) in the ultrahigh-pressure region is to construct Hugoniot curves using these isotherms and then to compare such Hugoniot curves with experimentally determined points.

The Mie-Grüneisen EOS (Ref. 16) cannot be used in this high-pressure region, as its use assumes that neither the ion nor the electron thermal contributions are important. Since both of the above thermal contributions must be added to the 0-K isotherm in order to obtain a proper Hugoniot curve, the problem arises as to which thermal models are the most appropriate in the region of interest.

The ion thermal contribution to the EOS was calculated using the Debye-Grüneisen perfect-gas interpolation method.[17,18] This method does not include a detailed treatment of phase transitions. However, up to the GPa region (35 GPa for lead and 330 GPa for Mo, for example) it has been found by others[19] that satisfactory results are obtained for the Hugoniot curves without considering phase transitions at all. For higher pressure values, the fluid phase, which becomes the most significant, is taken into account using the method of Ref. 18.

The EOS obtained with the above model, as well as with any other ion fluid theory, depends on the values of the Grüneisen coefficient Γ, which in turn is related to the cold compression curve by means of the following expression:[5]

$$\Gamma(V)=\frac{t-2}{3}-\frac{V}{2}\frac{\partial^2(P_cV^{2t/3})}{\partial V^2}\Big/\frac{\partial(P_cV^{2t/3})}{\partial V}\ . \tag{12}$$

Several authors have found that various values of t correspond to different configurations of the crystal cell. Thus, $t=0$, 1, and 2 give, respectively, the Slater-Landau[16] (SL) ionic crystal state, DM (Ref. 14) linearly aligned metal atoms, and Vaschenko-Zubarev[20] free volume (FV) expressions. More recently, it was proposed by Romain *et al.*[21] to generalize the interpretation of τ_g as being a characteristic parameter of each material. In terms of the compression variable η, Eq. (12) may be expressed as

$$\Gamma(\eta)=-\frac{1}{3}\tau_g+\frac{1}{2}\frac{\eta^2\dfrac{\partial^2P_c}{\partial\eta^2}+\frac{2}{9}[1-\tau_g(1+2\tau_g)]P_c}{\eta\dfrac{\partial P_c}{\partial\eta}-\frac{2}{3}(1+\tau_g)P_c}\ , \tag{13}$$

where

$$\tau_g=t-1\ .$$

For $\eta=1$, one obtains the boundary condition in Eq. (6). The value of τ_g may be obtained for each material by comparing experimental shock-wave data to theoretical calculations based on Eq. (13). This last equation relates the ion thermal excitations to the cold compression curve and emphasizes the interdependence between these two components of the EOS.

In contrast, the electron thermal contribution cannot readily be described by a single theory, valid for all material elements and for all ranges of temperature and compression. Since a thorough study of this topic is beyond the scope of this paper, we have restricted our calculations to those elements whose electron thermal contributions to the EOS can be reasonably described by one of several available thermodynamic theories.

The Thomas-Fermi-Khirzhnits (TFK) model is considered to give the most realistic formulation of the statistical behavior of the isolated atom and in addition, there are available tables of scaled values of computed thermodynamic functions based on this model.[22] In order

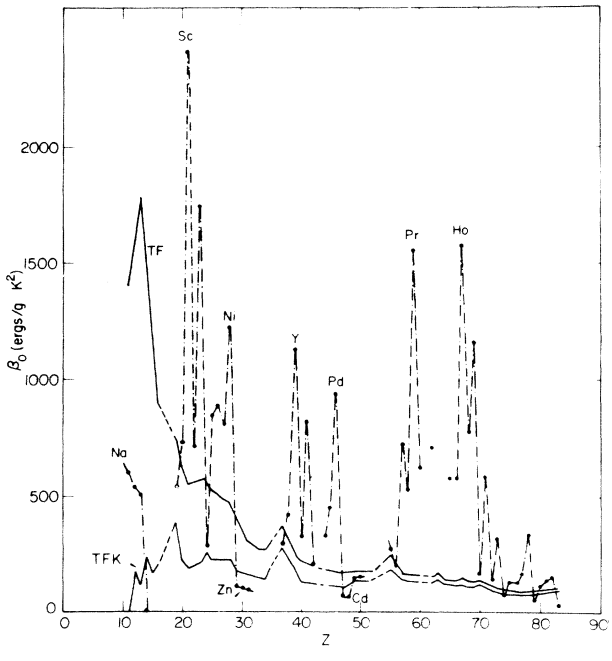

FIG. 1. Plots of electronic specific heat β_0 as a function of atomic number Z for various elements. Calculated values of the TF and TFK models are shown as well as experimental points taken from Ref. 28. Regions in the calculated curves where no data are available are marked by a dashed line. —·—·—·, lines connecting adjacent experimental points.

TABLE I. Summary of physical properties and interpolation parameters used in cold compression curve calculations for seven metals.

Element	Z	V_0 (Å^3)	B_0 (GPa)	Γ_0	τ_g	η_1	η_2
Al	13	215.71	75.036	2.14	−1		
Cd	48	1035.64	48.605	2.29	0	1.273	2.710
Cu	29	342.62	136.15	2.00	0.5		
Fe	26	307.15	109	2.15	1		
Mo	42	655.94	269	1.63	−1		
Pb	82	2487.64	42.353	2.38	0	1.476	2.125
W	74	1174.29	308	1.68	−1		

to investigate the range of applicability of the TFK model, the electronic specific heat β_0 was obtained using the tables in Ref. 22 and compared with the experimental results for material elements of various values of Z, the atomic number. The results are shown in Fig. 1.

It can readily be seen that the effect of the shell structure, which is neglected in the statistical models, has an important influence on these results for most of the elements of the Periodic Table. Certain elements such as Cd and W appear to be affected to a much smaller extent and therefore the calculated β_0 values are quite close to the experimental ones.

When shell-structure effects are small, though not negligible, the use of a numerical interpolation between the Saha [local thermodynamic equilibrium (LTE)] and the TFK methods appear to yield satisfactory results.[23] It is also possible to perform EOS calculations which take shell structure into account as for example by using Liberman's average-atom (AA) model (INFERNO).[24] Results of such calculations for Al, Cu, and Mo are available in the literature.[11]

In calculating the theoretical Hugoniot curves for the elements considered in this paper, it was found that the TFK theory gave the best results except for the case of molybdenum where the INFERNO results were adopted.

IV. RESULTS

In Table I are listed the physical properties and interpolation parameters for calculating the cold compression curves of seven metals investigated in this paper, using the phenomenological model presented here.

In Figs. 2 and 3 the calculated 0-K isotherms and Hugoniot curves for Cd and W are shown. Also shown are experimental points collected from the literature. Those experimental data that are indicated with their error bars originate from impedance-matching experiments. These require for their interpretation the use of a standard EOS model and the different shaped points indicated in the figures have been determined using different EOS models. In Fig. 3 there are added curves obtained from the SESAME tables for tungsten. As can be seen, the agree-

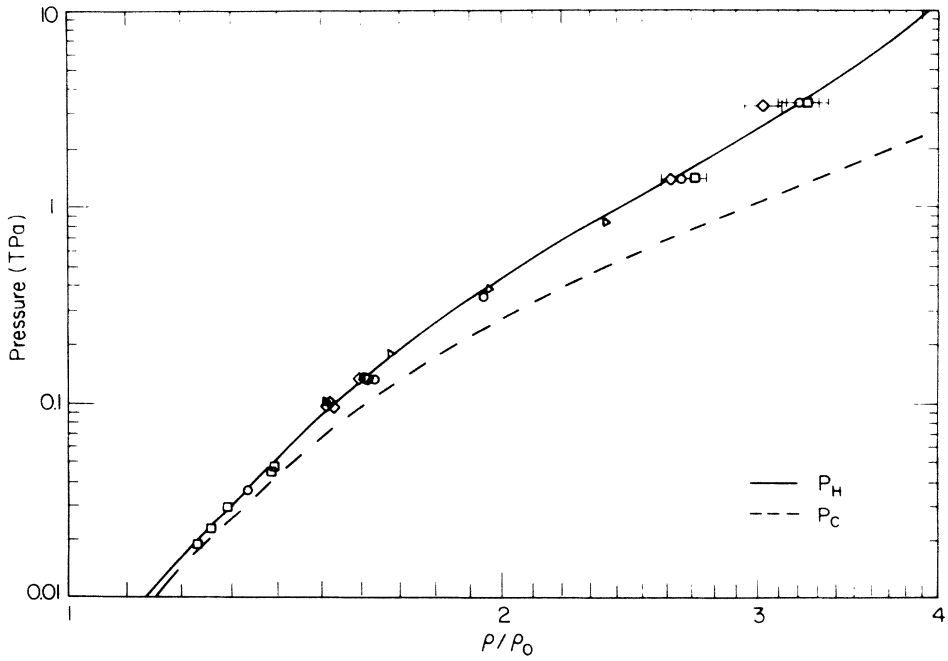

FIG. 2. Zero-degree-Kelvin isotherm and Hugoniot curve for Cd. Experimental points taken from □, Ref. 29; ○, Ref. 30; ◇, Ref. 19; and ▷, Ref. 32. Data with error bars originate in impedance-matching experiments of Cu-Cd stack from Ref. 31 interpreted by use of different Cu EOS: ⊢□⊣, present work; ⊢○⊣, SESAME table no. 3331; ⊢◇⊣, SESAME table no. 3332.

ment with experiment is excellent over the whole range of compression values. In the case of tungsten, the results of our calculations seem to give a somewhat better agreement with experiment than the SESAME results (which are based on the Barnes model).

The results of similar calculations are shown for Pb in Fig. 4. The need for a revision of the EOS for this metal has already been indicated by Ragan in a recent paper.[10] This is due to an apparent inconsistency between the Pb and the Mo EOS SESAME tables (material no. 3200 and no. 2981, respectively) used by him in interpreting his impedance-matching experiments. Incidentally, this Mo table uses the Saha-TFK interpolation to calculate the electron thermal contribution. Ragan therefore concludes that the lead Hugoniot curve needs to be "softer" than predicted by the Pb SESAME table, even though this would increase the discrepancy in the results of a similar experiment using a lead-quartz stack. Our calculations using the TFK model appear to confirm these results of Ragan and show that, if the above-mentioned SESAME tables are used, the resulting Hugoniot curve is just at the edge of the experimental error bar. On the other hand, if the latest SESAME table for Mo (no. 2983), which incorporates Liberman's self-consistent-field model for the electron thermal contribution, or our proposed EOS for Mo, are used, a better agreement is obtained.

The results of our calculations of the Hugoniot curves for Mo are shown in Fig. 5. In the same figure we show, for comparison, the Hugoniot curves derived from the above-mentioned SESAME tables for Mo, namely, no. 2981 and no. 2983. It is seen that the first of these fits the experimental values at low compression while the second gives a better fit for higher compressions. Our curve, which has been calculated using the AA-predicted values for the electron thermal contribution, appears to give a proper interpolation between the two extremes.

In Figs. 6 and 7 are shown the results obtained for Al and Cu.

Finally, in Fig. 8 the calculations carried out for Fe are presented. The application of our model to iron is complicated by the existence of several solid-state phase transitions for this element. In our calculations we consider only the ϵ phase which is stable above 25 GPa. Here we can no longer use for Γ_0 and B_0 in Eq. (8) and (9) the experimental values measured in the normal state, but we use instead quantities extrapolated from measurements in the solid phase of interest. For example, Γ_0 is deduced from the slope of the U_s-U_p (shock vs particle velocities) curve obtained from compiled shock-wave data[25] while B_0 values have been fitted so as to give good agreement with the experimental Hugoniot curve. Our theoretical prediction of the Hugoniot curve in Fig. 7 makes use of the TFK model for the electron thermal contribution. The observed discrepancy between the experimental Hugoniot points and the calculated curve above a compression of 1.8 is not surprising if we take into account the large difference between the experimental and calculated values of the electronic specific heat β_0 as shown in Fig. 1. Nevertheless, our curve is still closer to the experimental data in that region than the Hugoniot curve obtained from the Fe SESAME table (no. 2140) which is based on the TFD model. Since it is known that the TFD model gives values of the electron thermal contribution which are greater than those obtained using the TFK theory and

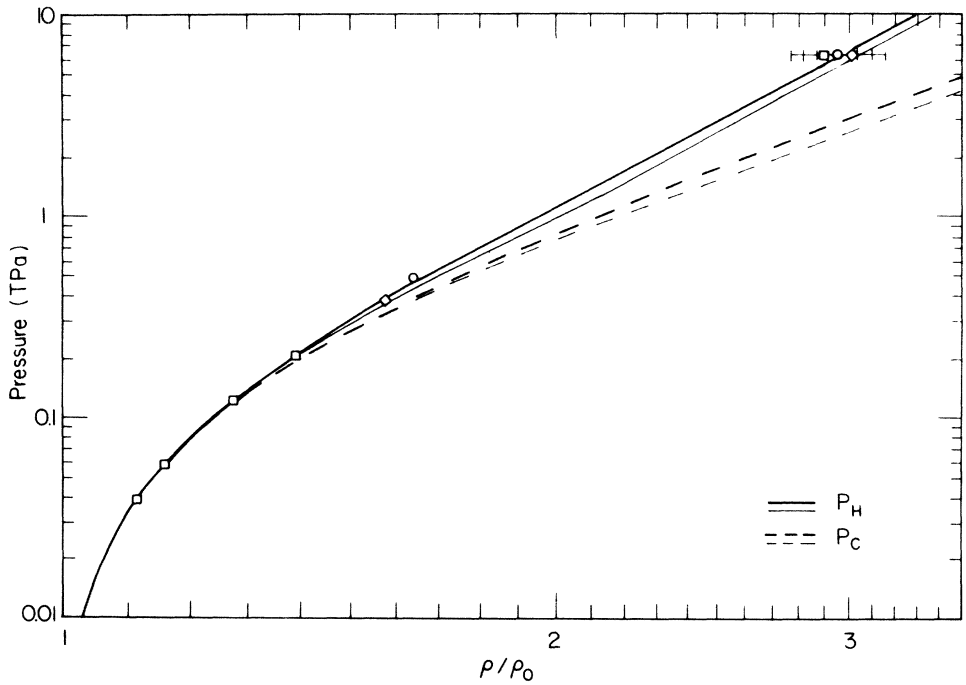

FIG. 3. Comparison of zero-degree-Kelvin isotherms and Hugoniot curves in W. Heavy line shows present work and light line the results derived from SESAME table no. 3451. Experimental points taken from □, Ref. 19; ◇, Ref. 34; ○, Ref. 35. Data with error bars were derived from impedance-matching experiments of Mo-W stack (Ref. 10) using different Mo EOS: ⊢□⊣, present work; ⊢○⊣, SESAME table no. 2981; ⊢◇⊣, SESAME table no. 2983.

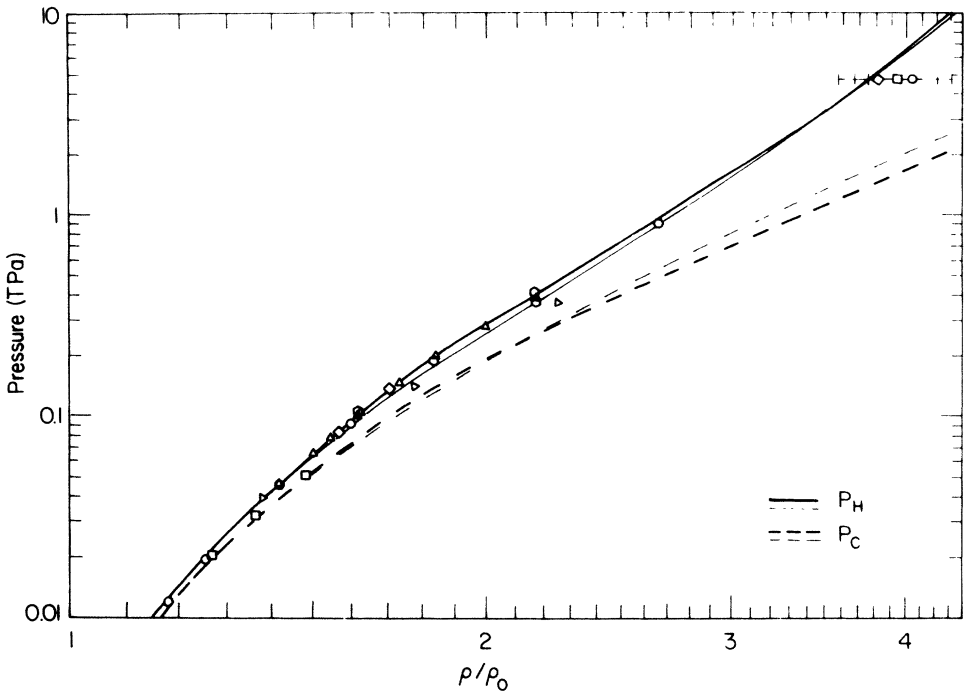

FIG. 4. Comparison of zero-degree-Kelvin isotherms and Hugoniot curves in Pb. Heavy line shows present work and light line the computations derived from SESAME table no. 3200. Experimental points taken from ○, Ref. 25; □, Ref. 29; ▷, Ref. 30; △, Ref. 36; ◇, Ref. 19; ⬯, Ref. 37; ⬭, Ref. 32. Data with error bars originate in impedance-matching experiments of a Mo-Pb pair from Ref. 10 using different Mo EOS: ⊢□⊣ , present work; ⊢○⊣ , SESAME table no. 2981; ⊢◇⊣ , SESAME table no. 2983.

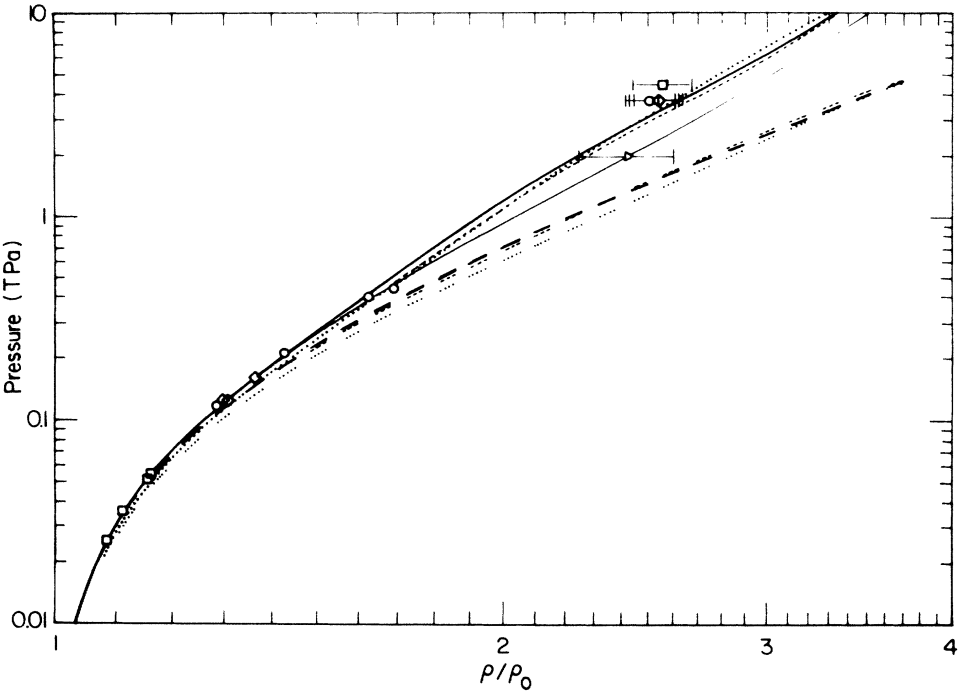

FIG. 5. Comparison of zero-degree-Kelvin isotherms and Hugoniot curves in Mo. Present results of the cold compression curve as well as those obtained from the Barnes model are represented by the dashed line (———); augmented-plane-wave (APW) (--- ---) and AA (· · · · · · · ·) predictions are also shown. The respective calculated Hugoniot curves are indicated by a heavy solid line (present result), light solid line (SESAME table no. 2980), dashed line (SESAME table no. 2981), and dotted line (SESAME table no. 2983). Experimental points taken from □, Ref. 29; ○, Ref. 38; ◇, Ref. 19; ⊢▷⊣ , Ref. 39. Data originating in impedance-matching experiments of a Pb-Mo pair from Ref. 10 using our Pb EOS is indicated by ⊢□⊣ . Results derived from similar experiments on a Al-Mo stack (Ref. 10) using different Al EOS: ⊢◁⊣ , present work; ⊢○⊣ , SESAME table no. 3712; ⊢◇⊣ , SESAME table no. 3713.

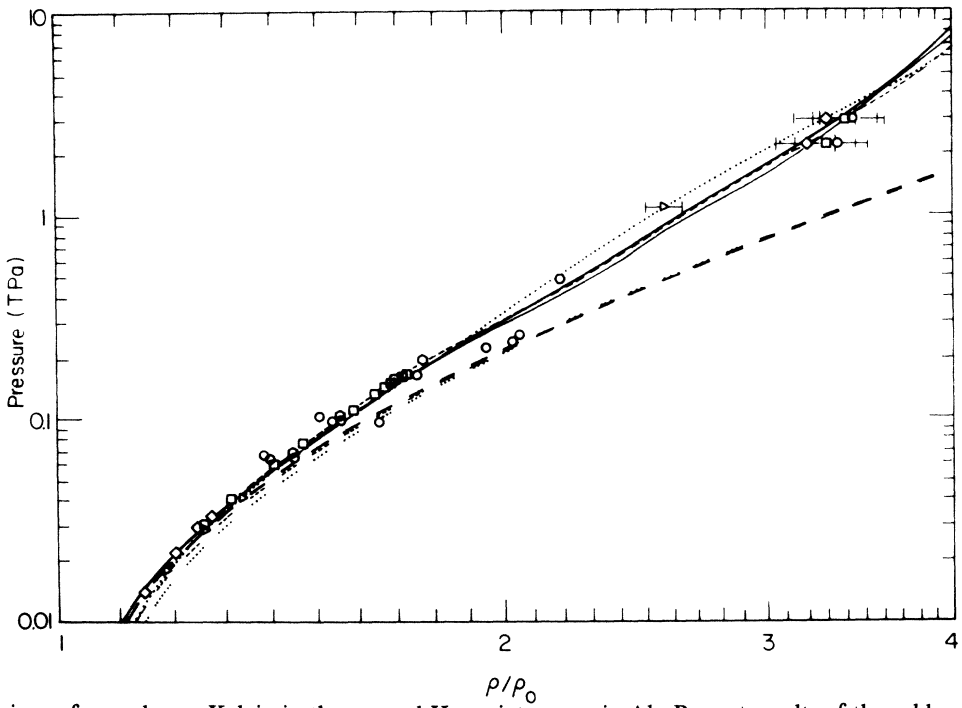

FIG. 6. Comparison of zero-degree-Kelvin isotherms and Hugoniot curves in Al. Present results of the cold compression curve as well as those obtained from the Barnes model are represented by the dashed line (———); APW (--- ---) and AA (· · · · · · · ·) predictions are also shown. The respective calculated Hugoniot curves are indicated by a heavy solid line (present results), light solid line (SESAME table no. 3710), dashed line (SESAME table no. 3712), and dotted line (SESAME table no. 3713). Experimental points taken from ◇, Ref. 31; ▷, Ref. 40; □, Ref. 41; ○, Ref. 42; o , Ref. 37; o , Ref. 43; ⊢▷⊣, Ref. 44. Data originated in impedance-matching experiments of Mo-Al stacks from Refs. 1 and 10 using different Mo EOS: ⊢□⊣, present work; ⊢○⊣, SESAME table no. 2981; ⊢◇⊣, SESAME table no. 2983.

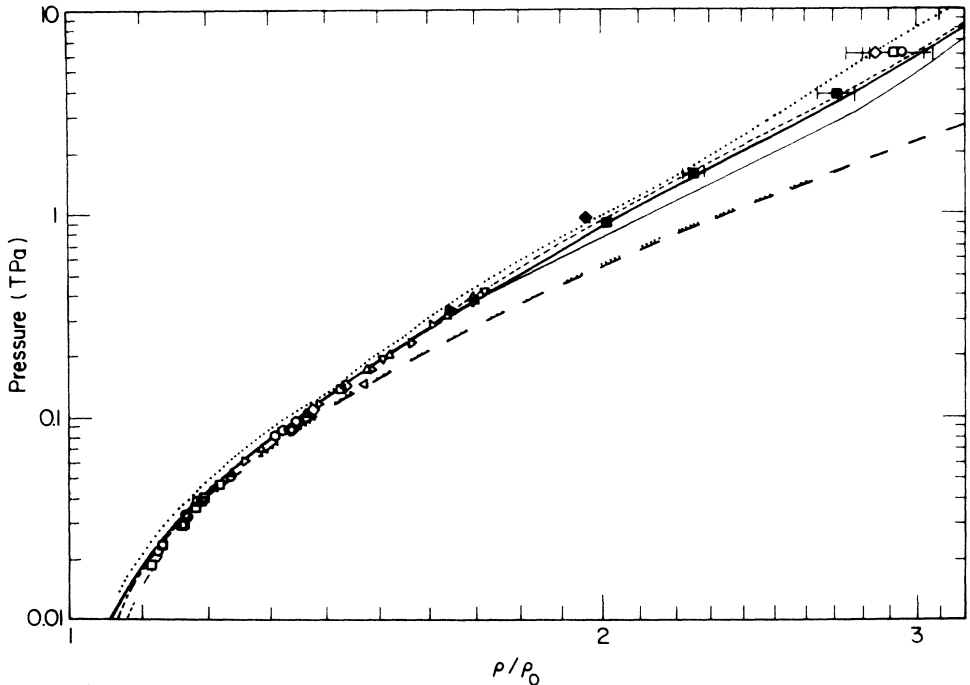

FIG. 7. Comparison of zero-degree-Kelvin isotherms and Hugoniot curves in Cu. Present results of the cold compression curve as well as those obtained from the Barnes model are represented by the dashed line (———); APW (--- ---) and AA (· · · · · · · ·) predictions are also shown. The respective calculated Hugoniot curves are indicated by a heavy solid line (present results), light solid line (SESAME table no. 3330), dashed line (SESAME table no. 3331), and dotted line (SESAME table no. 3332). Experimental points taken from □, Ref. 31; ○, Ref. 29; ▷, Ref. 41; ◁, Ref. 7; △, Ref. 36; ▽, Ref. 37; o , Ref. 25; ◇, Ref. 19; ◆, Ref. 43; ■, Ref. 32. Data originated in impedance-matching experiments of Pb—Cu pairs from Ref. 33 interpreted by our Pb EOS are indicated by ⊢■⊣. Results derived from similar experiments on a Mo-Cu stack (Ref. 1) using different Cu EOS: ⊢□⊣, present work; ⊢○⊣, SESAME table no. 2981; ⊢◇⊣, SESAME table no. 2983.

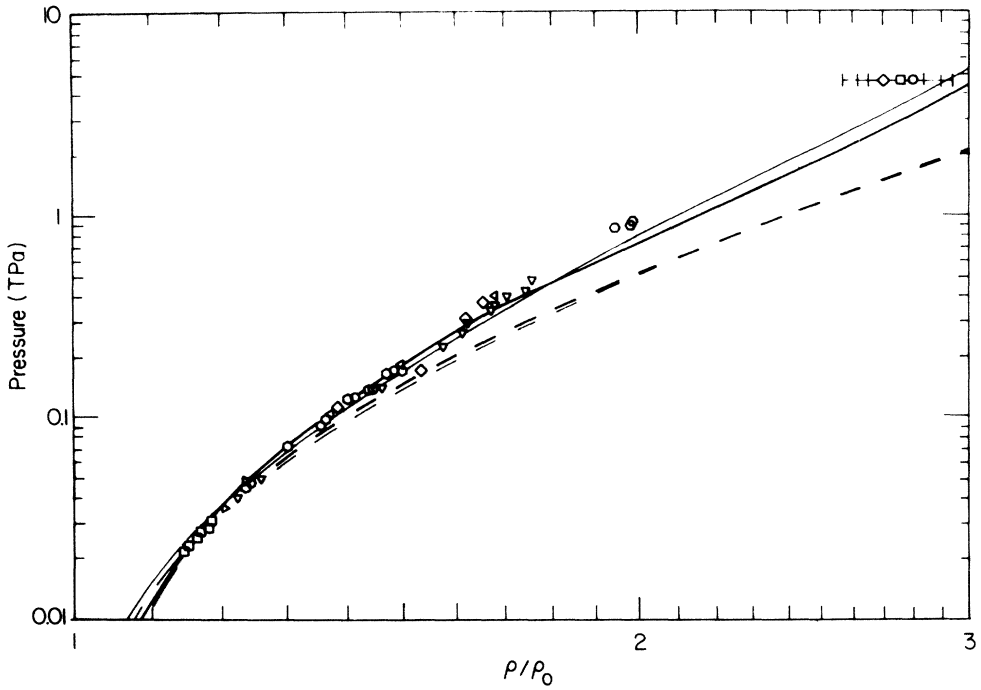

FIG. 8. Comparison of zero-degree-Kelvin isotherms and Hugoniot curves in Fe. Light line shows present work and heavy line the results derived from SESAME table no. 2140. Experimental points taken from □, Ref. 25; ▷, Ref. 29; ◁, Ref. 45; ○, Ref. 25; ○, Ref. 19; ◇, Ref. 37; ◁, Ref. 42; , Ref. 38. Data with error bars originate in impedance-matching experiments of a Mo-Fe pair from Ref. 1 using different Mo EOS: ⊢□⊣, present work; ⊢○⊣, SESAME table no. 2981; ⊢◇⊣, SESAME table no. 2983.

since, as can be seen in the figure, the cold compression curves are almost identical, we are led to the conclusion that the ion thermal contributions have not been properly calculated in the iron SESAME tables.

V. DISCUSSION

One consequence of our model for the cold compression curve may be that it can provide an accurate estimate of the nuclear Grüneisen coefficient Γ. The connection between this coefficient and the cold compression curve is given by Eqs. (12) and (13).

In Fig. 9 we show a comparison between different theoretical calculations and experimental measurements of this parameter for Al. The fitted value of τ_g for Al in our work is $\tau_g = -1$, indicating that for this element the SL configuration seems to be valid, in agreement with other works.[5,18] The theoretical curve calculated by the phonon theory of Godwal *et al.*,[26] as well as that given by the SL expression obtained from Eq. (12) using a 0-K isotherm taken from the same reference, are shown in the figure. Also shown is the curve calculated from Eq. (13) using the cold compression curve as obtained from our calculations. All these curves are compared to Neal's experimental points.[27] In addition, we show the normal value Γ_0 for Al in the figure. As can be seen, our calculations fit this normal value better than either of the other theoretical predictions, as well as being about as good as they in the remainder of the range.

Of the elements studied in this paper, only for Pb and Cd have the experimental values published to date reached the pressure range in which the Morse-QSM interpolation technique is required. This is probably due to the fact

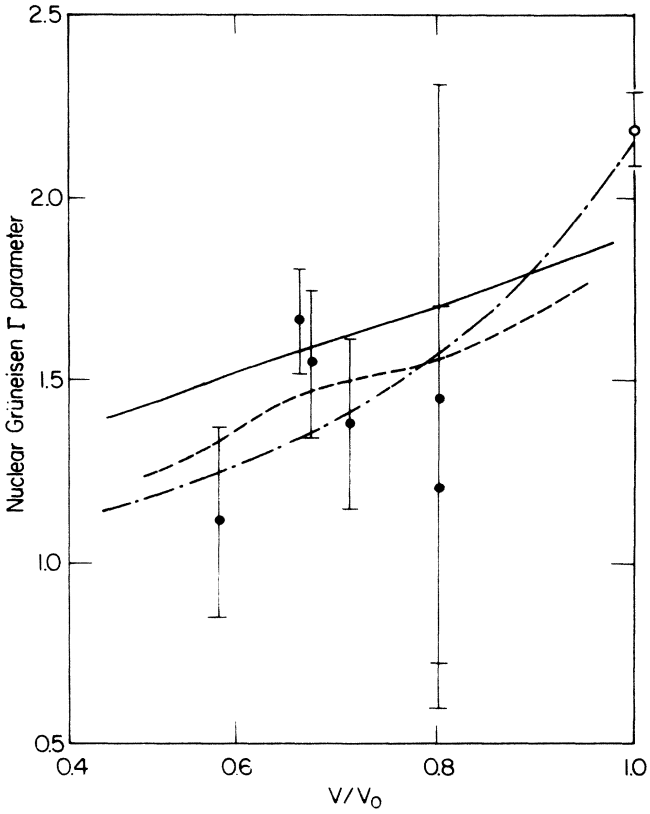

FIG. 9. Plot of nuclear Gruneisen Γ parameter vs volume compression ratio (V/V_0) for Al. Experimental values taken from Ref. 27 ● and Ref. 28 ○. Theoretical curves indicated by solid and dashed lines as obtained from Ref. 26. Present results are indicated by —·—·—·.

that these elements have closed (or nearly closed) shells which are characterized by a comparatively uniform electron density distribution as assumed by the QSM theory. Incidentally, Sn may be another element which fits into the same category but the Hugoniot data presently available is not sufficient to permit the construction of a reliable fit. For the other cases studied here the use of the pressure correction term derived from the Morse diatomic potential is sufficient to give a proper fit to the experimental data published to date.

In conclusion, we have shown that the cold compression curve can be calculated in a straightforward manner provided that the values of B_0, Γ_0, and τ_g are known. We have applied this model to a number of elements and have found excellent agreement with both experiment and more sophisticated theoretical computations. It is our belief that this formulation can be extended to other metals not considered here and, in a modified version, perhaps to compounds and alloys as well.

[1]C. E. Ragan III, Phys. Rev. A **29**, 1391 (1984).

[2]N. C. Holmes, R. J. Trainor, R. A. Andersen, V. T. Lee, D. L. Banner, E. M. Campbell, R. J. Harrach, W. C. Mead, R. J. Olness, D. W. Phillion, M. D. Rosen, F. Ze, and R. E. Turner, in *High Pressure in Research and Industry*, edited by C. M. Backman, T. Johanisson, and L. Tegner (Arkitektkopia ISBN, Uppsala, 1982), Vol. 1, p. 164.

[3]F. Cottet, J. P. Romain, R. Fabbro, and B. Faral, Phys. Rev. Lett. **52**, 1884 (1984).

[4]R. S. Hawke, IEEE Trans. Nucl. Sci. **NS-28**, 1542 (1981).

[5]B. K. Godwal, S. K. Sikka, and R. Chidambaram, Phys. Rep. **102**, 121 (1983).

[6]B. I. Bennett, J. D. Johnson, G. I. Kerley, and G. T. Rood, Los Alamos National Laboratory Report No. LA-7130, 1978 (unpublished).

[7]J. F. Barnes, Phys. Rev. **153**, 269 (1967).

[8]R. D. Cowan and J. Ashkin, Phys. Rev. **105**, 144 (1957).

[9]C. E. Ragan III, Phys. Rev. A **21**, 458 (1980).

[10]C. E. Ragan III, Phys. Rev. A **25**, 3360 (1982).

[11]Los Alamos Scientific Laboratory Report No. LASL-79-62, 1980, edited by N. G. Cooper (unpublished).

[12]N. N. Kalitkin and L. V. Kuz'mina, Fiz. Tverd. Tela (Leningrad) **13**, 2314 (1971) [Sov. Phys.—Solid State **13**, 1938 (1972)].

[13]R. M. More, Phys. Rev. A **19**, 1234 (1979).

[14]J. S. Dugdale and D. K. C. MacDonald, Phys. Rev. **89**, 832 (1953).

[15]D. A. Khirzhnits, Zh. Eksp. Teor. Fiz **32**, 115 (1957) [Sov. Phys.—JETP **5**, 64 (1957)].

[16]J. C. Slater, *Introduction to Chemical Physics* (McGraw-Hill, New York, 1939).

[17]S. B. Kormer, A. I. Funtikov, V. D. Urlin and A. N. Kolesnikova, Zh. Eksp. Teor. Fiz. **42**, 686 (1962) [Sov. Phys.—JETP **15**, 477 (1962)].

[18]S. L. Thompson and H. S. Lauson, Sandia Corporation Livermore Report No. SC-RR-710714, 1972 (unpublished).

[19]R. G. McQueen and S. P. Marsh, J. Appl. Phys. **31**, 1253 (1960).

[20]V. Ya. Vaschenko and V. N. Zubarev, Fiz. Tverd. Tela (Leningrad) **5**, 886 (1963) [Sov. Phys.—Solid State **5**, 653 (1963)].

[21]P. Romain, A. Migault, and J. Jacquesson, *High Pressure Science and Technology*, edited by K. D. Timmerhaus and M. S. Barber (Plenum, New York, 1979), Vol. I, p. 99.

[22]S. L. McCarthy, Lawrence Livermore Laboratory Report No. UCRL-14364, 1965 (unpublished).

[23]K. S. Trainor, J. Appl. Phys. **54**, 2372 (1983).

[24]D. Liberman, Phys. Rev. B **20**, 4981 (1979).

[25]M. Van Thiel, Lawrence Livermore Laboratory Report No. UCRL-50108, 1967 (unpublished).

[26]B. K. Godwal, S. K. Sikka, and R. Chidambaram, Phys. Rev. B **20**, 2362 (1979).

[27]T. Neal, Phys. Rev. B **14**, 5172 (1976).

[28]K. A. Gschneider, *Solid State Physics—Advances in Research and Applications* (Academic, New York, 1964), Vol. 12, p. 275.

[29]J. M. Walsh, M. H. Rice, R. G. McQueen, and F. L. Yarger, Phys. Rev. **108**, 196 (1957).

[30]L. V. Al'tshuler, K. K. Krupnikov, and M. I. Brazhnik, Zh. Eksp. Teor. Fiz. **34**, 886 (1958) [Sov. Phys.—JETP **7**, 614 (1958)].

[31]J. M. Walsh and R. H. Christian, Phys. Rev. **97**, 1544 (1955).

[32]L. V. Al'tshuler, A. A. Bakanova, and R. F. Trunin, Zh. Eksp. Teor. Fiz. **42**, 91 (1962) [Sov. Phys.—JETP **15**, 65 (1962)].

[33]R. F. Trunin, M. A. Podurets, B. N. Moiseev, G. V. Simakov, and L. V. Popov, Zh. Eksp. Teor. Fiz. **56**, 1172 (1969) [Sov. Phys.—JETP **29**, 630 (1969)]; **62**, 1043 (1972) [**35**, 550 (1972)].

[34]A. H. Jones, W. M. Isbell, and C. J. Maiden, J. Appl. Phys. **17**, 3493 (1966).

[35]K. K. Krupnikov, M. I. Brazhnik, and V. P. Krupnikova, Zh. Eksp. Teor. Fiz. **42**, 675 (1962) [Sov. Phys.—JETP **15**, 470 (1962)].

[36]L. V. Al'tshuler, S. B. Kormer, M. I. Brazhnik, L. A. Vladimirov, M. P. Speranskaya, and A. I. Funtikov, Zh. Eksp. Teor. Fiz. **38**, 1061 (1960) [Sov. Phys.—JETP **11**, 766 (1960)].

[37]L. V. Al'tshuler, S. B. Kormer, A. A. Bakanova, and R. F. Trunin, Zh. Eksp. Teor. Fiz. **38**, 790 (1960) [Sov. Phys.—JETP **11**, 573 (1960)].

[38]K. K. Krupnikov, A. A. Bakanova, M. I. Brazhnik, and R. F. Trunin, Dokl. Akad. Nauk SSSR **148**, 1302 (1963) [Sov. Phys.—Dokl. **8**, 205 (1963)].

[39]C. E. Ragan, M. G. Silbert, and B. C. Diven, J. Appl. Phys. **48**, 2860 (1977).

[40]M. H. Rice, R. G. McQueen and J. M. Walsh, *Solid State Physics—Advances in Research and Applications* (Academic, New York, 1958), Vol. 6, p. 1.

[41]A. C. Mitchell and W. J. Nellis, J. Appl. Phys. **52**, 3363 (1981).

[42]I. C. Skidmore and E. Morris, *Proceedings of the Symposium on Thermodynamics of Nuclear Materials* (IAEE, Vienna, 1962), p. 173.

[43]S. B. Kormer, A. I. Funtikov, V. D. Urlin, and A. N. Kolesnikova, Zh. Eksp. Teor. Fiz. **42**, 686 (1962) [Sov. Phys.—JETP **15**, 477 (1962)].

[44]A. P. Volkov, N. P. Voloshin, A. S. Vladimirov, V. N. Nogin, and V. A. Simonenkov, Pis'ma Zh. Eksp. Teor. Fiz. **31**, 623 (1980) [JETP Lett. **31**, 588 (1980)].

[45]L. V. Al'tshuler, K. K. Krupnikov, B. N. Ledenev, V. I. Zhuchikhin, and M. I. Brazhnik, Zh. Eksp. Teor. Fiz. **34**, 874 (1958) [Sov. Phys.—JETP **34**, 606 (1958)].